RUL Predict of IGBT Based on DeepAR Using Transient Switch Features

Jianwen Ge [1], Yixiang Huang[2], Zhiyu Tao[3], Bingchu Li[4], Dengyu Xiao[5], Yanming Li[6], and Chengliang Liu[7]

[1,2,3,5,6,7]School of Mechanical Engineering of Shanghai Jiao Tong University
Minhang, Shanghai, 200240, China
gejianwen@sjtu.edu.cn
huang.yixiang@sjtu.edu.cn
515020910236@sjtu.edu.cn
xiaodengyu@sjtu.edu.cn
ymli@sjtu.edu.cn
chlliu@sjtu.edu.cn
[4]School of Mechanical Engineering of University of Shanghai for Science and Technology
Yangpu, Shanghai, 200090, China
bcli@sjtu.edu.cn

ABSTRACT

The insulated gate bipolar transformer (IGBT) has been widely used in power electrical system such as wind power converter and drive converter. However, the high load and capricious working environment make IGBT become the most vulnerable component in the electrical system. In this paper, a method based on probabilistic forecasting with auto-regressive recurrent networks (DeepAR) is proposed to predict the remaining useful life (RUL) of IGBT. Firstly, the transient data of the collector-emitter voltage signal are acquired when IGBT is turned off. Then, the different characteristics are extracted from transient data and the features that can represent the health state of IGBT best are chosen as the input of the DeepAR model to predict the remaining life of IGBT. Experiment results show that the log-log ratio of transient data can be an accurate precursor to predict RUL, and compared with other similar series predict models such as Auto-Regressive Integrated Moving Average (ARIMA) and Simple Exponential Smoothing (SES), DeepAR can get higher accuracy.

1. INTRODUCTION

The insulated gate bipolar transformer (IGBT) of which technology has developed rapidly in recent decades becomes an ideal switching device in the field of power electronics. Nowadays, the latest generation of IGBT not only has the advantages of high input impedance, low control power, simple driving circuit, high switching speed and low switching loss that are the superiorities of Metal-Oxide-Semiconductor Field-Effect Transistor (MOSFET) but also has the advantages of high current density, low saturation voltage and strong current processing ability that are the distinguishing features of the bipolar power transistor. In application scenarios of high voltage, high current, and high frequency, IGBT has incomparable performance with other power devices. Therefore, wind power converters in wind energy conversion and drive converters in electric vehicles mainly use IGBT as power devices.

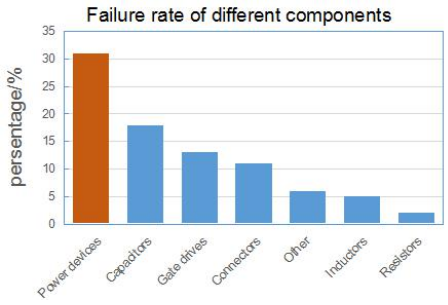

Figure 1.The failure rate of different electrical components

However, IGBT working under high voltage and high current still have the problems of large internal resistance, large conduction consumption, and poor anti-interference and anti-shock capabilities. IGBT is likely to over-heat and over-voltage during operation. The statistical analysis of the reliability of industrial electronic devices shows that the power devices are the components that are most likely to fail in the electronic and electrical system (Yang, Bryant, Mawby, Xiang, Ran, & Tavner, 2011). The failure of IGBT will lead to the paralysis of the entire electrical system, the

chain reaction of which may destroy the system and other related components. In many cases, the entire equipment will be shut down. Later-site cleaning and equipment maintenance may cost a lot of manpower and material resources, resulting in huge economic losses. Therefore, it is urgent to build a reliable IGBT diagnosis system that uses the intelligent diagnosis technology to predict the life of IGBT and to aid maintenance.

More and more researchers explore the failure mechanism of IGBT and propose various methods to predict RUL. At present, approaches mainly used to predict RUL of IGBT can be classified into three categories: the finite element analysis (FEA) approaches based on the energy method, the analytic approaches based on empirical Coffin-Manson formula, and the data-driven approaches based on aging precursor parameters. FEA approaches use the finite element model to analyze the damage energy which is generated by stress and strain on each temperature cycle and will gradually accumulate and finally bring about material fatigue(Basaran & Chandaroy, 1997; Plekhov, Saintier, Palin-Luc, Uvarov, & Naimark, 2007). Thébaud, Woirgard, Zardini, Azzopardi, Briat, and Vinassa (2003) established a non-linear finite element simulation model to simulate the dissipated energy in solder to predict the failure of IGBT based on the energy theory that this part of the energy will act on the interior of the material and cause fatigue damage in each temperature cycle. Astigarraga, Ibanez, Galarza, Echeverria, Unanue, Baraldi, and Zio (2016) and Ali, Dusmez, and Akin (2016) used IGBT modules of different manufacturers and models for aging life test. They found that under the same test conditions, the final failure modes of different modules were different and the changing trends of gate current, gate voltage, and collector voltage of different modules varied from module to module. These results indicate that when the internal parameters of IGBT are different, the actual aging proceedings and results will be significantly different. Therefore, FEA approaches can perform a conductive role in predicting RUL of IGBT module, but the result of FEA may be imprecise in practical conditions where the temperature and current in IGBT are variable and parameters of structural dimension and material are difficult to obtain accurately. The analytic approaches predict RUL based on coffin-Manson fatigue theory that the number of temperature aging cycles of materials is exponentially related to the junction temperature swing ΔT_j. Therefore, researchers conduct many aging tests under different temperature swings to find the analytical formula between RUL and temperature to predict the life of IGBT. Schilling, Schäfer, Mainka, Thoben, and Sauerland (2012) used the multiple aging data obtained under different conditions to find out the relationship between the aging times and the swing of temperature according to the traditional coffin Manson method, which was proved to be a capable method to predict the remaining life. However, the analytic method needs a large number of experiments to ensure the accuracy of the result, which will take a large amount of time.

It is a more reliable and practical method to find an effective precursor parameter to reflect the aging degree and predict the remaining life of IGBT. Hence, researchers have done many experiments and figured out different aging precursor parameters. Patil, Celaya, Das, Goebel, and Pecht (2009) monitored many physical quantities in the aging process and found that the threshold voltage of the gate increased, the collector-emitter voltage (V_{CE}) decreased, and the capacity voltage curve translates to left, which meant that there was positive trapped charge in IGBT. Guastavino, Dardano, and Torello (2008) measured the partial discharge characteristic of IGBT working on the specific PWM mode and found out the relationship between the residual life and the partial discharge characteristic. Smet, Forest, Huselstein, Richardeau, Khatir, Lefebvre, and Berkani (2011) set different temperature swings and maximum temperature to execute accelerated aging experiments and found that V_{CE} increases with the number of aging in cases of bond wire fracture and falling off and there is no obvious change in V_{CE} in other failure modes. Zhou, Zhou, and Sun (2013) collected V_{CE}, gate emitter voltage (V_{GE}) and gate current (I_g) in IGBT aging process with high-precision and high sampling rate oscilloscope, and found that chip defect would lead to the change of transient I_g waveform which then is used to determine whether IGBT is aging. Alghassi, Perinpanayagam, Samie, and Sreenuch (2015) found that V_{CE} gradually increased with the increase of aging times, so the experimental data were divided into different stages according to the data aging and then a statistical method was established to predict the remaining life. Liu Liu, Mei, Zeng, Yang, and Zhou (2017) also found that V_{CE} increased with the aging times, but the measured voltage fluctuated greatly, which means there was large noise. For this reason, an improved extreme learning machine model was proposed to predict the remaining life, which achieved better results than other similar algorithms.

Most of the studies mentioned above estimate the aging degree of IGBT based on the change of on-state V_{CE} which is generally convinced to increase when the bonding wire falls off or the solder layer is fatigued. However, little attention has been focused on the change of switching transient waveform. It can be feasible to use on-state V_{CE} as an aging precursor to predict RUL under laboratory environments where constant current and temperature swing are guaranteed. However, on-state V_{CE} is affected by the internal temperature and conduction current which usually changes unpredictably under the actual complex conditions. When the bond wire or solder layer fails, the transient waveform will reflect these changes more directly because the internal electrical characteristics change. In this paper, we use the transient waveform of IGBT at the moment of switching as the aging index to predict RUL. Firstly, instantaneous wave-forms when IGBT switches off are

intercepted from the V_{CE} signal collected by the signal acquisition system. Then the characteristics of the waveform are extracted and fed to DeepAR (Salinas, Flunkert, Gasthaus, & Januschowski, 2019) after the appropriate filtering to predict the changing trend. When the characteristics exceed a threshold value, IGBT is considered invalid and the prediction of the residual life can be calculated. Also, a simulation of the IGBT transient waveform is conducted to figure out which parameter changes.

2. DEGRADATION MECHANISM OF IGBT

In this section, we will introduce the aging mechanism of IGBT. Firstly, the internal structure of IGBT is introduced and then an equivalent circuit is proposed based on IGBT configuration. Secondly, the transient characteristics of current and voltage in turn off time are analyzed according to the equivalent circuit of IGBT. Finally, the aging failure mechanism of IGBT is explained and the change of the turn-off transient curve is discussed in the aging process from the perspective of the aging mechanism, to provide the basis for predicting the life with the transient waveform.

2.1. IGBT structure

IGBT is a composite power semiconductor device that can be regarded as a Darlington structure composed of bipolar junction transistor (BJT) and MOSFET. IGBT is designed as a multi-cell structure. Many small cells are integrated into one piece of semiconductor.

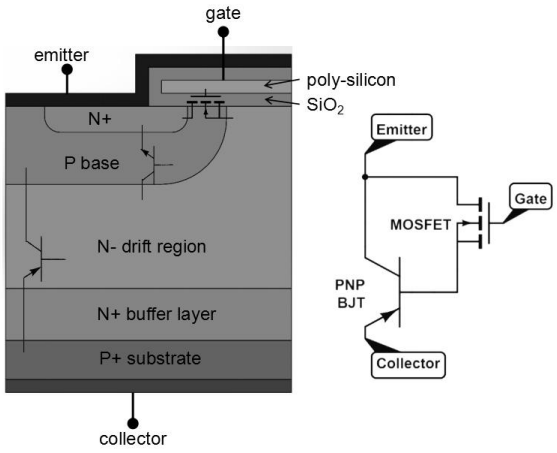

(a) (b)

Figure 2. IGBT structure (a) and equivalent circuit of IGBT (b).

The configuration of one IGBT cell (see Figure 2(a)) are very similar to MOSFET, that is, adding a P+ substrate layer on the drain of MOSFET as the collector of IGBT. In Figure 2(a), P + and N + denote that the collector and source regions are heavily doped, and N- denotes that the base doping concentration is low. As is shown in Figure 2(b), the equivalent circuit diagram of the field terminated IGBT is given according to its structure. The N+ region, gate, and N-region are equivalent to a MOSFET. P region, N-region, and P+ region form a PNP transistor. When sufficient voltage is applied to the gate of IGBT, a large number of electrons gather between the P area and the gate to form an inversion layer, so the MOSFET is turned on. After that, the IGBT is turned on due to the current flowing through the PNP type BJT connected with the collector.

2.2. IGBT transient characteristics

In order to analyze the dynamic characteristics of IGBT, the internal capacitance and inductance of IGBT should be analyzed firstly. There is no structure similar to inductance in the microstructure of IGBT, so we can ignore the internal inductance and focus on the analysis of capacitance. The gate structure is illustrated in detail in Figure 3, which helps analyze the main capacitance of IGBT.

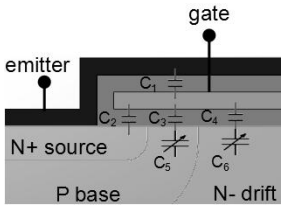

Figure 3. Capacitance in IGBT.

As shown in Figure 3, the gate capacitance can be divided into two parts: gate-emitter capacitance C_{GE} and gate-collector capacitance C_{GC}. C_{GE}, which also is described as input capacitance, consists of gate-emitter metal capacitance C_1, gate-N+ region capacitance C_2, and gate-P region capacitance C_{GP} composed of C_3 and C_5 which changes with gate emitter voltage (V_{GE}). Known as Miller capacitance, C_{GC} is composed of C_4 and C_6, which varies with V_{CE}.

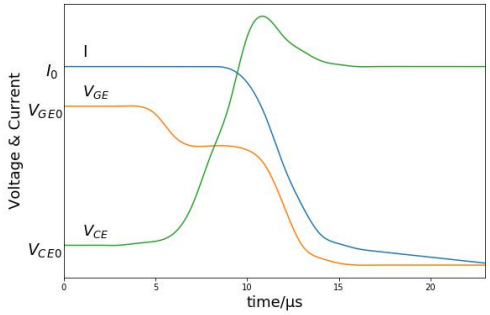

Figure 4. Transient waveform when IGBT is turned off.

The equivalent circuit composed of a PNP BJT and an N-channel MOSFET can be used to analyze the shutdown process. BJT is a current-controlled device, which is controlled by MOSFET drain current as depicted in Figure 2(b). MOSFET connected with the base of BJT is a voltage-controlled device that is driven by V_{GE}. In the shutdown process, V_{GE} first drops to the Miller platform because C_{GE} and C_{CG} discharge. Then V_{GE} remains constant until V_{CE} rises to the source voltage when C_{CG} completes discharge.

Since V_{GE} is still greater than the threshold voltage of MOSFET, collector-emitter current does not drop. After the end of the Miller platform, MOSFET is turned off, and the current decreases. An induced voltage is generated by the inductance of the load circuit during current diminution, which accounts for the peak of V_{CE}. Finally, the peak voltage is absorbed by integrated diode and V_{GE} and the current dwindle slowly to zero.

2.3. Degradation mechanism

The main failure mode of IGBT is fatigue failure resulting from thermal stress. The coefficients of thermal expansion of materials inside the IGBT module are different. When the chip is heated, the thermal expansion of different material layers will vary from each other and the thermal-mechanical stress consequently generated will change with the change of temperature, resulting in thermal fatigue damage and finally the device failure. The most common failure types of IGBT modules are bond wire lift and solder layer fatigue. Bond wires include gate bond wire and emitter bond wire, which are made of aluminum. The gate bond wire that only a small current I_g passes through is generally more durable. The bond wires of emitter usually are made up of several juxtaposed lead wires. But it is easy to break down because of greater heat generation and greater temperature change resulting from a great current. Although the resistance of the bonding wire is very small, when the bonding wire falls off or breaks, the emitter resistance will increase and the temperature rise caused by the bonding wire fault will further increase the emitter resistance. As for solder layer fatigue, there are two solder layers including the upper solder layer between the silicon chip and the DBC substrate and the lower solder layer between the DBC substrate and the copper substrate. The solder layer is a solder joint between the IGBT chip and the copper substrate that is connected with the collector of IGBT. When the solder layer fatigue occurs, the collector resistance will increase directly. In conclusion, the degradation of IGBT leads to a gradual increase in the collector resistance. Such resistance change is so subtle that it is difficult to measure the resistance change by common methods. However, in the moment of IGBT switch, the waveform of V_{CE} will amplify the influence of resistance change, which makes it possible for us to infer the resistance change by transient waveform. Ali, Ugur, and Akin (2019) compared the changing of the thermal resistance, on-state collector-emitter voltage, and the gate threshold voltage ($V_{g(th)}$), only to find $V_{g(th)}$ is the best indicator to evaluate the health status of the power converter. Also, it is impractical to measure $V_{g(th)}$ under working conditions. However, using the change of transient waveform caused by $V_{g(th)}$ to observe the status of the IGBT module is more feasible. A transient simulation is conducted to further discuss the parameter change in section 5.2.

3. PROGNOSTIC APPROACH

3.1. Kalman Filter

Kalman filter is a commonly used filtering algorithm to reduce signal noise from acquired data. Compared with other filtering algorithms, Kalman filter has higher accuracy and better interpretability in the field of signal processing. Kalman filter is essentially an algorithm applied to estimate a linear system state. The algorithm assumes that the object of the signal acquisition is a linear system, whose output is determined by the state variables and initial values. In the process of signal acquisition, there are errors in the actual state and output due to sensor errors. Therefore, the acquisition system can be described as follows:

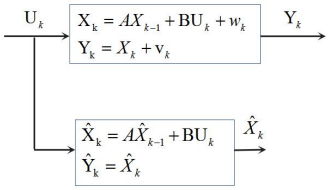

Figure 5. Kalman filter model

Where X_k is the system state which represents the real signal. Y_k is the observed state representing data acquired by sensors . U_k is the initial state of the system. $\hat{X}_k$ is the estimated value of X_k. A is the system matrix and B is the observation matrix. The output matrix is regarded as a unit matrix in this data acquisition system. $w_k \sim (0, \Sigma_p)$ and $v_k = \mathrm{err}(Y_k) \sim (0, \Sigma_{err})$ are process noise and measurement noise which are both assumed to be Gaussian distribution with covariances Σ_{err} and Σ_p respectively.

In order to attain an optimal estimation of the real signal X_k, the distribution of the observed value Y_k and the estimated value $\hat{X}_k$ are combined to get a more accurate distribution of X_k. Because of measurement noise and process noise, the distribution of Y_k and $\hat{X}_k$ can be described as follow:

$$Y_k \sim (Y_k, \Sigma_{err}) \tag{1}$$

$$\hat{X}_k \sim (\hat{X}_k, \Sigma_k) \tag{2}$$

Where Σ_k is estimation covariance, which is defined by Σ_{k-1} and Σ_p :

$$\Sigma_k = A\Sigma_{k-1}A^{\mathrm{T}} + \Sigma_p \tag{3}$$

Therefore, the optimal estimation distribution can be calculated using the formula:

$$\hat{X}_{opt} \sim \left(\hat{X}_k + K\left(Y_k - \hat{X}_k\right), \Sigma_{opt}\right) \tag{4}$$

Where K is the Kalman coefficient, which is defined as follow:

$$K = \Sigma_k \left(\Sigma_k + \Sigma_{err}\right)^{-1} \tag{5}$$

Finally, the expectation of Gaussian distribution is the optimal estimation. By conducting the Kalman filter, all points of sensor data can be updated by the estimation values that contain less noise.

3.2. LSTM

Long short-term memory network (LSTM) is one of the most widely used recurrent neural networks (RNN). RNN can get better results than traditional methods when processing a series of data,. However, with the increase of the number of layers, the neural network will have the problem of gradient disappearance and gradient explosion, so that the RNN of multiple layers cannot get a satisfying result. By properly designing memory cell, LSTM makes the network avoid decreasing gradient or exploding gradient, and makes the network have the characteristics of long-term memory.

3.3. Likelihood Function

The likelihood function $L(\theta|x)$ is a function of parameters. In statistics, the random variable x obeys a distribution with the parameter θ . With different parameters, the probability of random variable corresponding to the same value is also different. In general, the distribution with specific parameters is used to calculate the probability of variable. While $L(\theta|x)$ is a function of the parameters by giving the probability of every event. It can be calculated using the following formula:

$$L(\theta|x) = P(x|\theta) \tag{6}$$

The likelihood function with a given input of x is equal to the probability of x with a given parameter of θ . What matters are the values of parameters under which the corresponding likelihood function gets the largest value, not the function values. So the likelihood function is mainly used to obtain the most reasonable value of parameters to estimate the distribution of x .

3.4. DeepAR

The task of series prediction is to predict the next m points $\{s_{t+1}, s_{t+2}, s_{t+3}, ..., s_{t+m}\}$ according to the previous points $\{s_1, s_2, s_3, ..., s_t\}$. In fact, the prediction of the latter points can be seen as finding the probability of different values of the latter points. The ones with the largest probability can be used as the prediction values, while the estimation interval under different confidence can also be given. Therefore, the series prediction problem can be regarded as the problem to calculate the following conditional distribution:

$$P(s_{t+1:T}|s_{1:t}, c_{1:T}) \tag{7}$$

Where $\{s_1, s_2, s_3, ..., s_t, ..., s_T\}$ is the series to be predicted. The value of the series before t is known and the value from t to T needs to be predicted. $\{c_1, c_2, c_3, ..., c_T\}$ is covariates which can be known when conducting prediction. For example, the operations of the system can be considered as covariates.

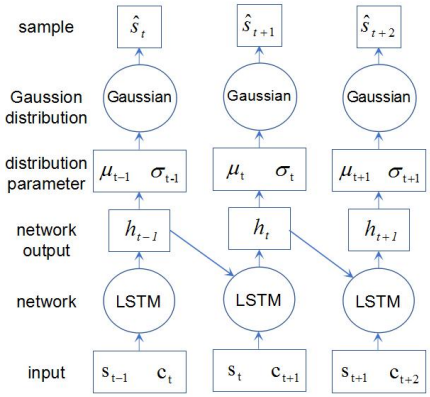

Figure 6.DeepAR training model

The training model is illustrated in Figure 6. Firstly, s_t and c_{t+1} are fed into a deep neural network LSTM one by one to generate a hidden layer h_t , which is used as a network input of next time. This calculation can be described as follow:

$$\mathbf{h_t} = f_{LSTM}(\mathbf{h_{t-1}}, s_t, \mathbf{c_{t+1}}, \mathbf{\Theta}) \tag{8}$$

Unlike most networks that regard h_t as prediction values of s_{t+1} , DeepAR uses h_t to generate a distribution, which then predicts s_{t+1} by sampling. Hence, we can generate the prediction of the next point $\hat{s}_{t+1}$ by conducting the following formulations:

$$\mu_t = \mathbf{w_\mu h_t} + b_\mu \tag{9}$$

$$\sigma_t = \log\left(1 + \exp\left(\mathbf{w}_\sigma \mathbf{h_t} + b_\sigma\right)\right) \tag{10}$$

$$P(s \mid \mu, \sigma) = \left(2\pi\sigma^2\right)^{-1/2} \exp\left(-(s-\mu)^2/(2\sigma^2)\right) \tag{11}$$

$$\hat{s}_{t+1} \sim P(s \mid \theta(\mathbf{h}_t, \mathbf{\Theta})) \tag{12}$$

Where $\mathbf{w}_\sigma, b_\sigma$ and $\mathbf{w}_\mu, b_\mu$ are parameters to be optimized to generate a Gaussian distribution of predict value $\hat{s}_{t+1}$. Since σ_t must be a number greater than zero, the formula generating σ_t from h_t uses a logarithmic function.

Finally, the difference between the sampled value $\hat{s}_{t+1}$ and the real value s_{t+1} is attained to calculate gradients of network parameters and distribution parameters. The maximum likelihood estimation algorithm is conducted to optimize the model:

$$L(s_{t+1:T}|s_{1:t}, c_{1:T}) = \prod_{t=t_0}^{T} P(s_t \mid \mathbf{h}_t, \boldsymbol{\Theta}) \tag{13}$$

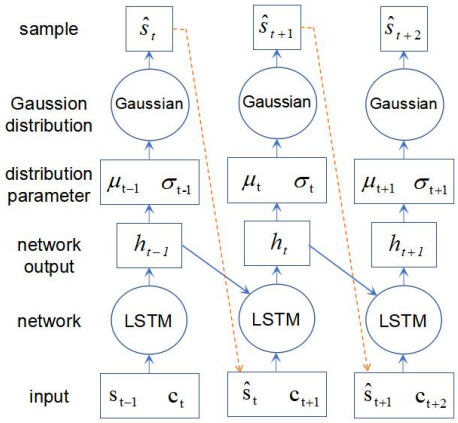

Figure 7.DeepAR prediction model

The prediction process is slightly different from the training process. In the training process, the network input of every time is actual s_{t+1}. However, $s_{t+1:T}$ is not known in the prediction, so the best prediction value generated from the previous prediction is fed into the prediction model to the next step prediction.

4. EXPERIMENT

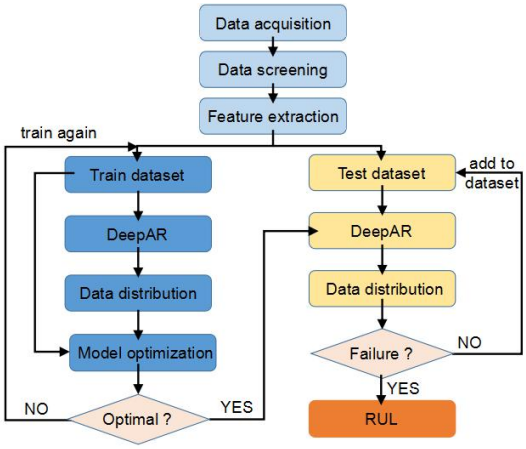

Figure 8. Flow diagram of proposed RUL prediction

In this section, we will give an overview of the whole process of RUL prediction (shown in Figure 8). Firstly, an accelerated aging test platform is established to obtain the data needed for life prediction. Secondly, data filtering, outliers deleting, and signal denoising are conducted to acquire the informative data we are interested in. After further feature extraction, data sets for residual life prediction are obtained. Then, we divide the data set into training data set and prediction data set, optimize the DeepAR model on the training set, and then use DeepAR on the test set for sequence prediction. Finally, the residual life is calculated according to the predicted results. All of these data processing details will be explained in the next few sections.

4.1. Data Source

In this article, the NASA IGBT aging dataset collected by Sonnenfeld, Goebel, and Celaya (2008) is used to validate the proposed algorithm. In the aging test, the discrete IGBT packages are operated at a temperature higher than its normal operating temperature to accelerate the aging of IGBT. The experimental platform not only collects the temperature of IGBT but also acquires the transient signals of the gate driving voltage V_{GS}, gate emitter voltage V_{GE} and collector-emitter voltage V_{CE} with a high-speed oscilloscope when switching.

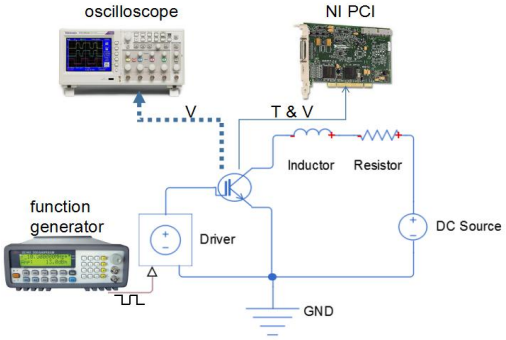

Figure 9. Circuit diagram of the aging platform

The acquisition circuit diagram of the test is shown in Figure 9. The device under test (DUT) used in the test is IGBT IRG4BC30KD encapsulated in TO220 with a rated voltage of 600V and a rated current of 15A. The load circuit uses a 4V stabilized voltage source to supply power. A resistance of 0.2 Ω is connected in series at the collector port of IGBT as the load. The driving circuit system is composed of Agilent 33220A function generator and the driving circuit board. The square wave signal generated by the function generator is adjusted by the driving circuit board and then input to the gate of IGBT. In the experiment, two different signal acquisition devices are applied to collect and monitor the status of IGBT. The first is a low-frequency signal acquisition system using NI PCI6229 as

the acquisition card. V_{GS}, V_{GE}, V_{CE}, and temperature are collected continuously at a lower frequency. Another set of acquisition system utilizes Agilent DSC6034 oscilloscope to collect high-frequency V_{GS}, V_{GE}, and V_{CE}. However, because of the excessive amount of high-frequency signal data, the oscilloscope can only be collected at intervals, about once every 25 seconds. Therefore, in this paper, we use the number of acquisition times to represent aging time.

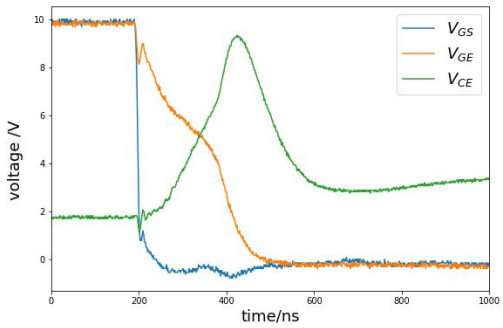

Figure 10. Transient signals

The data set provides an entire period date including on-state, off-state, and switching transient, which are collected at a 1GHz sampling rate. This paper mainly focuses on the turn-off transient signal that is shown in Figure 10. The driving voltage generated by the function generator is a standard square wave with a duty cycle of 40%. V_{GE} is the output of the driver circuit and is not a standard square wave because it is also affected by IGBT. V_{CE} measured is the potential difference between the collector and emitter of IGBT. The on-state V_{CE} voltage is determined by the input power supply, which is 4V in this experiment.

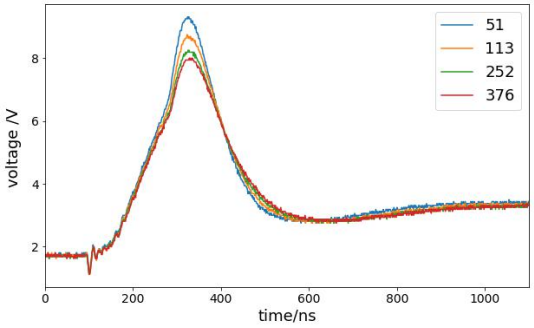

Figure 11. Transient waveforms of V_{CE} at different aging degree

In the aging process of IGBT, the change of IGBT internal structure will lead to the change of transient waveform. The waveform of V_{CE} voltage changes with aging time when IGBT is turned off, which has been mentioned in the paper. Figure 11 indicates that with the increase of aging time, the peak value of V_{CE} voltage decreases at the same temperature of 268 K. However, using the peak value of the voltage is not accurate enough for us to predict RUL of IGBT, which will be explained in the next section. Therefore, we need to further process the data to get the characteristic variables that can reflect the aging degree of IGBT.

4.2. Data Preparation

In the last section, we have figured out that the transient shutdown voltage of IGBT will change with aging time. Therefore, the main work of data preparation is to cut off the transient signal of IGBT from the collected data and extract a proper feature that can well represent the aging degree of IGBT.

First, the data at the moment when IGBT is turned off are cut off from the data collected by the oscilloscope. Most of the other data acquired when IGBT is in the off-state or on-state are useless because compared with the dynamic waveform signal at switching moment, these data are almost constant and contain little information. When analyzing the data, we also try to analyze the turn-on transient signal, but the turn-on signal is found no obvious change in the whole aging process. At the same time, through the analysis, we also discover that the driving voltage signal V_{GS} does not change with the aging degree and the V_{GE} signal will change slightly. Therefore, we finally intercept the turn-off transient signal of V_{CE} for subsequent analysis. At a temperature of about 268 K, the peak value of V_{CE} diminishes over time.

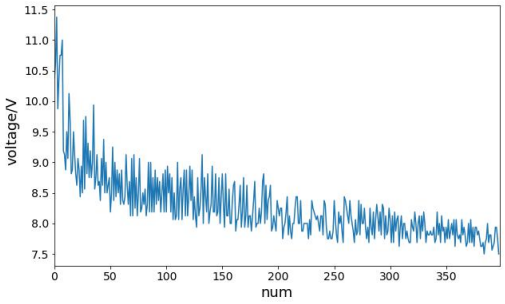

Figure 12. The peak voltage of V_{CE} over time

In Figure 12, it is depicted that with the increase of aging time, the peak value of V_{CE} shows a downward trend. But with a high fluctuating range, the peak voltage can not reflect the aging degree of IGBT.

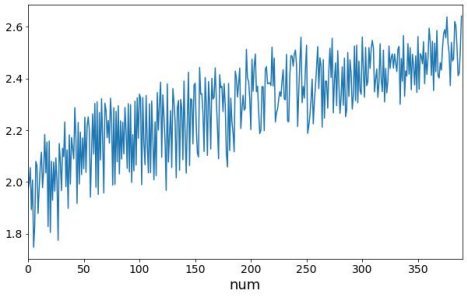

Figure 13.The log log ratio of V_{CE} over time

Therefore, we extract a feature that is more effective from the switching transient signals. Although the signal can also

be used as input directly, it is difficult to achieve the ideal effect because the amount of data is too small to train such a large model. Since the waveform of the V_{CE} signal at the moment of turning off will change with aging, a characteristic can be found to reflect the change of waveform. Through analysis and comparison, we find that the log log ration (LLR) is a good statistical feature to reflect the aging degree of IGBT. Compared with the peak value of V_{CE}, the noise interference component of LLR is significantly smaller than the aging trend component when IGBT is about to fail (shown in Figure 13). Other features, such as standard deviation and kurtosis, have similar trend changes to the peak, which will interfere with the prediction algorithm to find real failure time.

To get a better prediction of the remaining life, the extracted features need to be denoised. In the process of signal acquisition, noise is inevitable. After feature extraction, this noise is reflected on LLR, which is the reason for fluctuating as can be seen in Figure 13. Kalman filter is a commonly used filter to reduce the noise of a sensor signal. It has been proved to be an effective filter in dealing with bearing vibration signals (Qian, Yan, & Hu, 2014) and IGBT temperature(Eleffendi & Johnson, 2016). Therefore, the Kalman filter is harnessed in this paper to filter the signal before forecasting.

4.3. Series Prediction Based on DeepAR

After LLR is denoised, DeepAR is used to predict the trend of LLR regarded as a time series $s_{1:T}$. N data points $s_{T-N:T}$ before time t, which are assumed to be known, are used as input to predict M data $s_{T+1:T+M}$ after t time. DeepAR is essentially an auto-regressive model. Given $s_{T-N:T}$, s_{T+1} can be predicted. In this paper, the predicted s_{T+1} is used as the input to predict the value of the next time point T+2, and so on. Finally, the later M values can be predicted. As explained above (section 3.4), the output of DeepAR is actually a parameter of Gaussian distribution, so we can determine the 95% confidence interval of prediction. At the same time, the expected value of the distribution is the best prediction value.

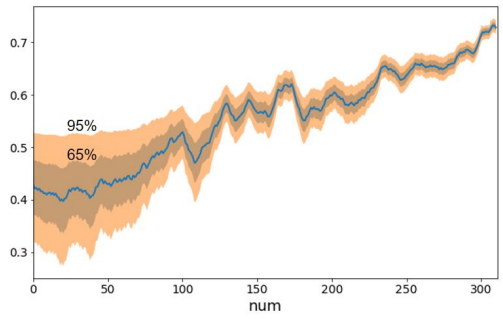

Figure 14. Prediction result of LLR

We use DeepAR to predict the next point by inputting the previous 50 points. Predict result is shown in Figure 14. With more data to train the model, DeepAR can get a better result. The interval of 95% confidence gets smaller and smaller as aging time increases.

4.4. RUL Estimation

According to the DeepAR prediction value, we can determine when the IGBT fails. The remaining life equals the time when the prediction value exceeds the threshold value minus the current time. If the series $s_{1:T}$ can represent the aging degree of the device, it can be judged as a device failure when s_i is greater than a threshold value $s_{threshold}$. Then the failure time is:

$$T_{fail} = \arg\min_i \{s_i > s_{threshold}\} \tag{14}$$

Using the auto-regressive model mentioned above, we can predict series values $s_{T+1:T+M}$ after the time point T_t . Then when the predicted value is greater than the threshold value, the predicted failure time T_{fail} is obtained. Therefore, the remaining life can be calculated by the following formula:

$$RUL = T_{fail} - T_t \tag{15}$$

In many fault diagnosis algorithms about life prediction, the algorithm only gives an optimal prediction value. However, this prediction value is affected by many factors, such as input data noise, model deviation, and working environment change of diagnosis object. Therefore, it is very important to give the reliability or uncertainty of the prediction value in the prediction algorithm. When using the DeepAR prediction sequence, we get a Gaussian distribution of the predicted value. According to the statistical principle, the interval within twice the standard deviation near the mean value is 95% confidence interval. Therefore, we can calculate the shortest life and the longest life at 95% confidence:

$$RUL_{\max} = T_{fail\,\max} - T_t \tag{16}$$

$$RUL_{\min} = T_{fail\,\min} - T_t \tag{17}$$

5. DISCUSSION

5.1. Prediction Horizon

In order to verify the effectiveness of the proposed method, we use the prediction horizon (PH) (Lei, Li, Guo, Li, Yan, & Lin, 2018) as the evaluation index to compare several commonly used algorithms such as ARIMA and SES. Prediction horizon is defined as:

$$PH = t_{EoL} - t_{i_{\alpha\beta}} \tag{18}$$

$$t_{i_{\alpha\beta}} = \min\{k \mid (k \in \Omega) \wedge (\pi(p(t_k))|_{-\alpha}^{+\alpha}) \geq \beta\} \tag{19}$$

Where $t_{i_{\alpha\beta}}$ is the time index when predictions first satisfy β-criterion for a given α; Ω is the set of all time indexes; t_k is the time index; β is the minimum acceptable probability mass; $p(t_k)$ is the predicted RUL distribution at the time t_k; t_{EoL} is the predicted End-of-Life; $\pi(p(l_{t_k}))|_{-\alpha}^{+\alpha}$ is the probability mass of the probability density function (PDF) within the α-bounds that are given by $\alpha^+ = r_* + \alpha \cdot t_{EoL}$ and $\alpha^- = r_* - \alpha \cdot t_{EoL}$ where r_* is the actual RUL.

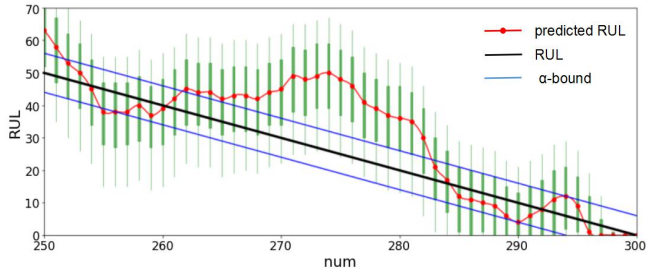

(a)

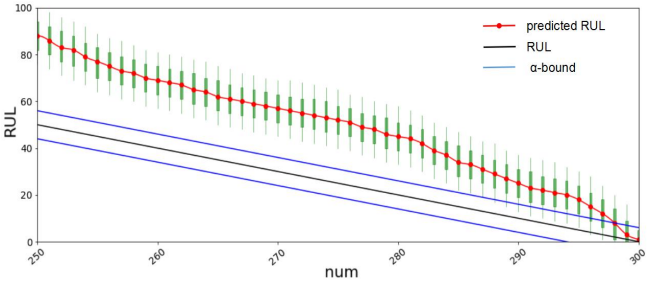

(b)

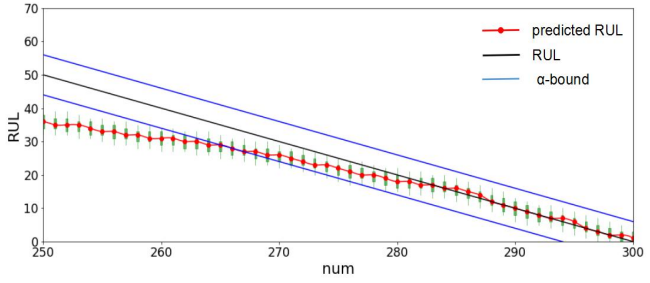

(c)

Figure 15. RUL predict of ARIMA (a), SES (b) and DeepAR(c)

To evaluate the effect of DeepAR, we set the PH parameter α to 0.02 and β to 0.5. The failure threshold is set to the average of LLR of the last ten times to calculate the predict RUL. As shown in Figure 15, the PH of DeepAR is 35, which means we are 95% sure to predict that IGBT will be failure 875 seconds before it is really broken-down. Compared with ARIMA and SES, DeepAR can not only get a higher PH but also narrower confidence interval which is shown in Figure 15 with green bars.

Table 1. Prediction horizon of different algorithms.

Algorithm	Prediction Horizon
ARIMA	17
SES	3
DeepAR	35

5.2. Transient Simulation

In order to further study the aging principle of IGBT, we use an improved Hefner model(Hefner Jr & Blackburn, 1988) to simulate the turn off transient of IGBT in this paper. The model regards IGBT as a composite of BJT and MOSFET and describes the transient process based on the bipolar transport principle and non-quasi-static approximation theory.

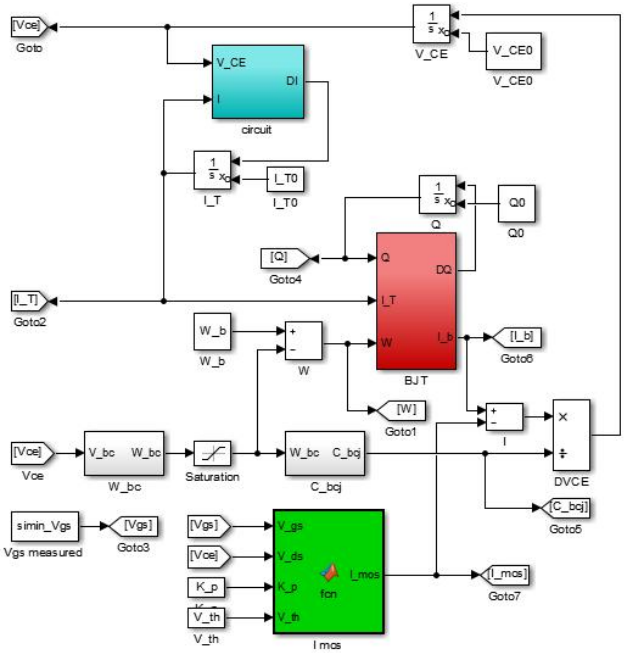

Figure 16.The simulation model of IGBT

In this paper, we use MATLAB/Simulink as the simulation platform to simulate IGBT devices. The simulation program can be divided into three parts: MOSFET, BJT, and the external circuit. The main parameters of the external circuit model are the resistance and inductance of the load circuit. When V_{CE} and I_T are input into the circuit model, the current change rate dI_T/dt is calculated. The BJT part is the

simulation of the PNP transistor in the IGBT structure (Figure 2), as shown in the red box in Figure 16. The MOSFET part simulates the corresponding MOSFET in the structure and calculates the current through the MOSFET according to the input V_{gs} and V_{ds}.

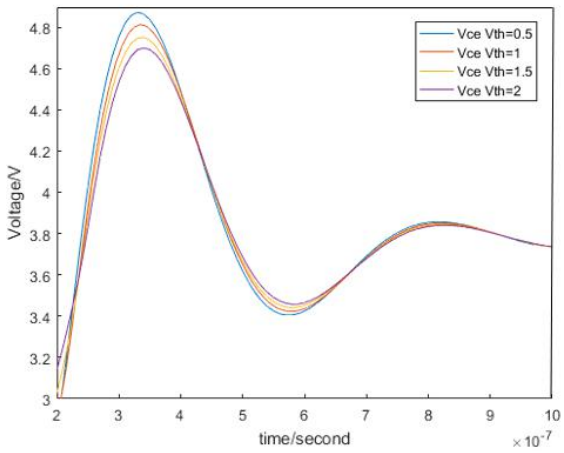

Figure 17.The Simulink result with different Vth

During the aging process of IGBT, obvious change of the V_{CE} waveform of switching off transient has been observed. To study the mechanism of blooming and to predict the remaining life, it is an innovative and significant method to find out the parameters changed in the aging process according to the transient model. First, a striking feature that can be seen by analyzing the IGBT aging data provided is that the peak value of the V_{CE} waveform would be significantly smaller during the aging process. Then, according to the change of the waveform, the parameters of the simulation model should also be changed to better fit the curve change. Through the simulation experiment, we find that when the threshold voltage (V_{th}) changes, the simulation output waveform has a similar change with the experimental results (shown in Figure 17).

V_{th} is the threshold voltage of MOSFET. The main factors affecting the threshold voltage are the thickness of the gate oxide, the doping concentration, and the temperature of the substrate. In the test, the temperature is controlled around 330K. Although the temperature will fluctuate during the test, the effect of temperature on the aging waveform is negligible. Therefore, we assume that the doping concentration of gate oxide and substrate changes with time.

6. CONCLUSION

This paper presents a method to predict the remaining life of IGBT by using the instantaneous waveform signal of V_{CE}. We extract LLR, the most characteristic feature of transient signal, which can reflect the change of aging degree, and use the DeepAR model to predict life after eliminating noise by Kalman filter. By comparing the results of SES and ARIMA, our algorithm can get the best results under the prediction horizon index. Finally, a modified Hefner model is established in MATLAB/Simulink to simulate the transient waveform, indicates that it is the change of V_{th} which leads to the variation of V_{CE}. Although it may take cost to acquire the transient signal in the actual working condition, our algorithm verifies the feasibility of using the transient signal to predict the remaining life. Moreover, by simulating the transient characteristic, more incisive and accurate degradation mechanisms can be fathomed to direct RUL prediction.

ACKNOWLEDGE

This project is supported by the National Key Technology R&D Program of China (No. 2017YFB1302004), and NSFC project (No. 51975356).

REFERENCE

Alghassi, A., Perinpanayagam, S., Samie, M., & Sreenuch, T. (2015). Computationally efficient, real-time, and embeddable prognostic techniques for power electronics. *IEEE Transactions on Power Electronics, 30*(5), 2623-2634. doi:10.1109/TPEL.2014.2360662

Ali, S. H., Dusmez, S., & Akin, B. (2016). *Investigation of collector emitter voltage characteristics in thermally stressed discrete IGBT devices.* Paper presented at the 2016 IEEE Energy Conversion Congress and Exposition, ECCE 2016.

Ali, S. H., Ugur, E., & Akin, B. (2019). Analysis of Vth Variations in IGBTs under thermal stress for improved condition monitoring in automotive power conversion systems. *IEEE Transactions on Vehicular Technology, 68*(1), 193-202. doi:10.1109/TVT.2018.2880993

Astigarraga, D., Ibanez, F. M., Galarza, A., Echeverria, J. M., Unanue, I., Baraldi, P., & Zio, E. (2016). Analysis of the Results of Accelerated Aging Tests in Insulated Gate Bipolar Transistors. *IEEE Transactions on Power Electronics, 31*(11), 7953-7962. doi:10.1109/TPEL.2015.2512923

Basaran, C., & Chandaroy, R. (1997). Finite element simulation of the temperature cycling tests. *IEEE Transactions on Components Packaging and Manufacturing Technology Part A, 20*(4), 530-536. doi:10.1109/95.650944

Eleffendi, M. A., & Johnson, C. M. (2016). Application of Kalman Filter to Estimate Junction Temperature in IGBT Power Modules. *IEEE Transactions on Power Electronics, 31*(2), 1576-1587. doi:10.1109/TPEL.2015.2418711

Guastavino, F., Dardano, A., & Torello, E. (2008). Measuring partial discharges under pulsed voltage conditions. *IEEE Transactions on Dielectrics and*

Electrical Insulation, 15(6), 1640-1648. doi:10.1109/TDEI.2008.4712668

Hefner Jr, A. R., & Blackburn, D. L. (1988). An analytical model for the steady-state and transient characteristics of the power insulated-gate bipolar transistor. *Solid State Electronics, 31*(10), 1513-1532. doi:10.1016/0038-1101(88)90025-1

Lei, Y., Li, N., Guo, L., Li, N., Yan, T., & Lin, J. (2018). Machinery health prognostics: A systematic review from data acquisition to RUL prediction. *Mechanical Systems and Signal Processing, 104*, 799-834. doi:10.1016/j.ymssp.2017.11.016

Liu, Z., Mei, W., Zeng, X., Yang, C., & Zhou, X. (2017). Remaining useful life estimation of insulated gate biploar transistors (IGBTS) based on a novel volterra K-nearest neighbor optimally pruned extreme learning machine (VKOPP) model using degradation data. *Sensors (Switzerland), 17*(11). doi:10.3390/s17112524

Patil, N., Celaya, J., Das, D., Goebel, K., & Pecht, M. (2009). Precursor parameter identification for insulated gate bipolar transistor (IGBT) prognostics. *IEEE Transactions on Reliability, 58*(2), 271-276. doi:10.1109/TR.2009.2020134

Plekhov, O. A., Saintier, N., Palin-Luc, T., Uvarov, S. V., & Naimark, O. B. (2007). Theoretical analysis, infrared and structural investigations of energy dissipation in metals under cyclic loading. *Materials Science and Engineering A, 462*(1-2), 367-369. doi:10.1016/j.msea.2006.02.462

Qian, Y., Yan, R., & Hu, S. (2014). Bearing degradation evaluation using recurrence quantification analysis and kalman filter. *IEEE Transactions on Instrumentation and Measurement, 63*(11), 2599-2610. doi:10.1109/TIM.2014.2313034

Salinas, D., Flunkert, V., Gasthaus, J., & Januschowski, T. (2019). DeepAR: Probabilistic forecasting with autoregressive recurrent networks. *International Journal of Forecasting*. doi:10.1016/j.ijforecast.2019.07.001

Schilling, O., Schäfer, M., Mainka, K., Thoben, M., & Sauerland, F. (2012). Power cycling testing and FE modelling focussed on Al wire bond fatigue in high power IGBT modules. *Microelectronics Reliability, 52*(9-10), 2347-2352. doi:10.1016/j.microrel.2012.06.095

Smet, V., Forest, F., Huselstein, J. J., Richardeau, F., Khatir, Z., Lefebvre, S., & Berkani, M. (2011). Ageing and failure modes of IGBT modules in high-temperature power cycling. *IEEE Transactions on Industrial Electronics, 58*(10), 4931-4941. doi:10.1109/TIE.2011.2114313

Sonnenfeld, G., Goebel, K., & Celaya, J. R. (2008). *An agile accelerated aging, characterization and scenario simulation system for gate controlled power transistors*.

Thébaud, J. M., Woirgard, E., Zardini, C., Azzopardi, S., Briat, O., & Vinassa, J. M. (2003). Strategy for designing accelerated aging tests to evaluate IGBT power modules lifetime in real operation mode. *IEEE Transactions on Components and Packaging Technologies, 26*(2), 429-438. doi:10.1109/TCAPT.2003.815112

Yang, S., Bryant, A., Mawby, P., Xiang, D., Ran, L., & Tavner, P. (2011). An industry-based survey of reliability in power electronic converters. *IEEE Transactions on Industry Applications, 47*(3), 1441-1451. doi:10.1109/TIA.2011.2124436

Zhou, S., Zhou, L., & Sun, P. (2013). Monitoring potential defects in an IGBT module based on dynamic changes of the gate current. *IEEE Transactions on Power Electronics, 28*(3), 1479-1487. doi:10.1109/TPEL.2012.2210249

BIOGRAPHIES

Jianwen Ge is a graduate student of Shanghai Jiao Tong University majoring in mechanical engineering. His main research interests include intelligent diagnosis and maintenance, remain useful life prediction of IGBT and machine learning.

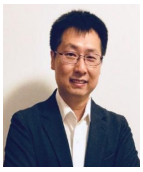

Yixiang Huang (M'14) received the B.S. in power and energy engineering in 2002, the M.S. and Ph.D. degrees in mechatronics engineering in 2006 and 2010, respectively, all from Shanghai Jiao Tong University, China. Currently, he is an Assistant Professor of Mechanical Engineering at Shanghai Jiao Tong University, China. Previously, he worked with the NSF Industry/University Cooperative Research Center for Intelligent Maintenance Systems at University of Cincinnati, USA. His current research interests include intelligent maintenance, prognostics and health management, big data analysis, sparse coding and dimensionality reduction for various industrial applications. He is a regular reviewer for a number of international journals.

Bingchu Li was born in Shandong, China, in 1988. He received the B.S. degree in mechanical engineering from Central South University, Hunan, China, in 2008, and the Ph.D. degree in mechanical engineering from Shanghai JiaoTong University, Shanghai, China, in 2019. He is currently an Assistant Professor of mechanical engineering at University of Shanghai for Science and Technology, Shanghai, China. His research interests include advanced control of nonlinear systems, switched reluctance motor drives with emphasis on vibration and acoustic noise elimination.